Acoustical characterization of perforated facings

L. Jaouen[a] and F.-X. Bécot
Matelys-Acoustique & Vibrations, 1 rue Baumer, 69120 Vaulx-en-Velin, France

(Received 13 January 2011; revised 13 January 2011; accepted 16 January 2011)

An experimental method to estimate the acoustical parameters of perforated facings used for noise control applications is proposed. These perforating facings (also called screens) can be woven or non-woven fabrics or even micro-perforated plates (MPP). Following the work by Atalla and Sgard [J. Sound Vib. **303**, 195–208 (2007)], the perforated facings are modeled as porous media composed with identical cylindrical perforations of circular cross-section. The acoustical parameters characterized with the proposed method are the radius of the perforations and the perforation rate (also named the open-porosity). These parameters are obtained from analytical expressions and a single measurement of the normal acoustic surface impedance of the perforated facing backed by an air cavity in a standing wave tube. The value of the static air flow resistivity can also be recovered with no additional assumption or measurement. In the case of a facing that contains perforations of an arbitrary shape, the radius parameter should be understood as a characteristic length of the visco-inertial dissipative effects. Results for two characterization examples (a low porosity screen and a high porosity one) are presented and discussed. Values of the estimated static air flow resistivity are compared with the results from direct measurements. Values of the predicted sound absorption coefficients are compared to the measured ones. © *2011 Acoustical Society of America*. [DOI: 10.1121/1.3552887]

PACS number(s): 43.58.Bh [KVH] Pages: 1400–1406

I. INTRODUCTION

Numerous passive noise control solutions use perforated facings (which will be called "screens" hereafter for the sake of simplicity) such as woven or non-woven fabrics or micro-perforated plates (MPP) for acoustical, mechanical protection, or even design purposes. Modeling the acoustical behavior of such thin porous elements, which are mainly used in addition with air gaps or other porous materials such as foams or fibrous materials, has been a research topic for several decades (see e.g., Refs. 1–6). In the work by Atalla and Sgard,[6] screens are modeled as porous media having rigid and motionless skeletons and composed by identical cylindrical perforations of circular cross-sections. In this work, a Johnson–Champoux–Allard (JCA) model[7,8] with a modified high frequency limit of the tortuosity is used to account for flow distorsions due to the perforations. Two independent unknown parameters are required to predict the acoustical behavior of a screen: the radius of the perforations r and the perforation rate ϕ. This latter parameter is equivalent to the open-porosity routinely used to describe porous media (see Ref. 9 for example). Any other combination of these two parameters can also be used. In particular the static air flow resistivity σ can also be used. Indeed, for a network of identical cylindrical perforations with circular cross-section σ is equal to $8\eta/(\phi r^2)$ where η is the dynamic viscosity of air.

From a practical point of view, it is usually difficult to directly measure the open-porosity of screens due to their small thicknesses with apparatus such as those described by Champoux *et al.*[10] or Leclaire *et al.*[11] To overcome this issue one can use arrangements of screen samples rather than only one sample. However, this may result in an increase of uncertainties for the measured open-porosity value due to the uncertainty increase on sample dimensions. Alternatively, an optical method can be used to assess the value of the open-porosity. Nevertheless such an optical estimation of the open-porosity is usually not easy for non-woven fabrics. Also, it is difficult to directly measure[12] static air flow resistances ($\sigma \times h$ where h is the thickness of the screen) lower than 50 N s m^{-3} due to low signal to noise ratios. The method presented in this paper proposes to overcome the issues mentioned above providing estimations of the open-porosity and of the static air flow resistivity σ (or static air flow resistance $\sigma \times h$) from the only measurement of the normal surface impedance of the screen backed by an air cavity in a standing impedance tube.

In the current work, the description of screens described by Atalla and Sgard is used: screens are modeled as porous media with rigid and motionless skeletons composed with identical cylindrical perforations of circular cross-section. The benefit of this type of modeling is the possibility to predict the screens performances via Transfer Matrix Method (TMM), Finite Element Method (FEM), or any technique which uses common acoustical porous models (with or without skeleton motion: limp,[13] rigid-body,[14] Biot[15,16]…) rather than adding a specific model to the technique.

Following Atalla and Sgard, two independent parameters among which the perforation radius r, the perforation rate ϕ, and the static air flow resistivity σ are sufficient to completely describe the acoustical behavior of a screen (i.e., for various acoustical excitation conditions such as diffuse field and for various configurations such as a screen + foam or fibrous materials + air cavity). We propose to assess r and ϕ from a measure of the normal acoustic surface impedance of the screen backed by an air cavity in a standing wave

[a]Author to whom correspondence should be addressed. Electronic mail: luc.jaouen@matelys.com

 0001-4966/2011/129(3)/1400/7/$30.00

tube. Estimations of these two parameters are obtained from analytical expressions and do not require any curve fitting. Note that for materials which are not composed with cylindrical perforations (e.g., usual woven fabrics), the radius of the perforations obtained from the characterization should be considered as a characteristic dimension describing the visco-inertial effects caused by the screen rather than a parameter describing the exact micro-structure of this screen.

The physical analysis and the model leading to the estimations of the screen parameters are presented in Sec. II. Finally, two characterization examples are reported to illustrate the method. These examples are discussed in Sec. III.

II. PHYSICAL ANALYSIS AND MODELING

Figure 1 presents a scheme of the experimental set-up. A screen of thickness h is clamped at its circumference in an impedance tube of radius R. Between the screen and the rigid backing lies an air gap of thickness d. For such conditions, measurements will be influenced by four phenomena. The first phenomenon corresponds to the visco-thermal dissipative effects inside the screen. These effects, mostly dominated by visco-inertial ones due to the small thickness of the screen, can be accurately modeled using the JCA model. The second phenomenon corresponds to the flow distortion effects generated on both sides of the screen which are not negligible compared to visco-thermal effects. These two phenomena are further discussed throughout this paper.

The two other phenomena influencing the screen response to a normal incidence plane wave: (i) acoustic resonances in the backing cavity and (ii) bending vibrations of the screen are briefly presented below.

(1) The acoustic modes in the backing cavity. Frequencies of these resonances are given in a first approximation by

$$f_{\text{cavity\_resonances}} = \frac{nc_0}{2d} \quad n \in \mathbb{N}^* \tag{1}$$

where n denotes the cavity mode number, $\mathbb{N}^*$ is the set of all natural numbers excluding zero, and c_0 is the speed of sound in air. This expression is obtained assuming the acoustic velocity is equal to zero at the screen-cavity interface ($x = -d$) and at the end of the tube ($x = 0$). To clearly identify these resonances, a minimum of five cavity modes is suggested. The number of these cavity modes n in the frequency range of use of a tube with a diameter $2 \times R$ can be computed as $n = d\beta_{1,0}/R$, where d denotes the cavity length. In this last expression, $\beta_{1,0}$ is the value for which $\pi \times \beta_{1,0}$ is the first positive zero of the first derivative of the Bessel function of the first kind and of order 1. An approximate value for $\beta_{1,0}$ is 0.59. Thus, for a 46 mm diameter impedance tube, a cavity length of 200 mm is required to observe five cavity modes.

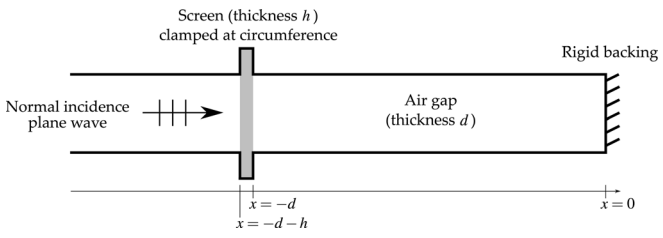

FIG. 1. Scheme of screen mounting conditions in an impedance tube for normal surface impedance measurements with a backing air gap.

(2) The bending vibrations of the screen, clamped at its circumference. Due to the cylindrical symmetry of the system (screen and air gap in the tube) and of the pressure field (plane wave at normal incidence), only bending modes (0, n) of the screen will be excited. Among all these symmetrical modes, mode (0, 1) is expected to have the highest magnitude. Modes which are not symmetrical might also be excited if clamped boundary conditions are not perfect or if the screen is not homogeneous. If the effect of the screen tension is neglected, the frequency of the first bending mode is (see Leissa[7] for example)

$$f_{1\text{st\_screen\_resonance}(0,\,1)} = \frac{1}{2\pi R^2}\sqrt{\frac{D}{\rho h}}\left(\lambda_0^1\right)^2 \tag{2}$$

where ρ denotes the mass density of the screen, D its flexural rigidity, and $(\lambda_0^1)^2$ is a parameter the value of which depends on the actual boundary conditions. For clamped boundary conditions, $(\lambda_0^1)^2 = 10.2158$. Leissa gives values of the parameter $(\lambda_i^j)^2$ for higher modes in Ref. 17 where i, here, denotes the number of nodal diameters and j denotes the number of nodal circles including the boundary circle.

Following the work by Atalla and Sgard,[6] the thin acoustical screen is considered as a rigid and motionless porous medium using the JCA model.[7,8] For material having identical and parallel cylindrical perforations with a circular cross-section, the five parameters of the JCA model can be expressed analytically as functions of r and ϕ (see Ref. 3). Four of these parameters are the static air flow resistivity $\sigma = 8\eta/(\phi r^2)$, the open-porosity ϕ, the characteristic viscous length $\Lambda = r$, and the characteristic thermal length $\Lambda' = r$. The expression of the fifth parameter, the high frequency limit of the dynamic tortuosity α_∞, is calculated from the works by Ingard[4] and Atalla and Sgard to account for flow distortion due to the screen perforations

$$\alpha_\infty = 1 + 2\frac{\varepsilon}{h} \tag{3}$$

with

$$\varepsilon = (1 - 1.13\xi - 0.09\xi^2 + 0.27\xi^3)\frac{8r}{3\pi} \quad \text{with} \quad \xi = 2\sqrt{\frac{\phi}{\pi}}, \tag{4}$$

ε is the corrected length accounting for flow distortions near the screen perforations. This expression is an approximation of the general expression given by Ingard valid for all values of the open-porosity ϕ contained in the range [0–1].

From the five parameters previously introduced, the screen dynamic mass density $\tilde{\rho}_{cs}$ and the screen dynamic bulk modulus $\tilde{K}_{cs}$ can be deduced using JCA model[7,8] (subscript cs stands for characteristic to the screen). These last intrinsic

material properties are related to the screen characteristic impedance Z_{cs} and the characteristic wave-number k_{cs} by

$$Z_{cs} = \sqrt{\tilde{\rho}_{cs}\tilde{K}_{cs}} \tag{5}$$

$$k_{cs} = \omega\sqrt{\frac{\tilde{\rho}_{cs}}{\tilde{K}_{cs}}} \tag{6}$$

Denoting Z_{ca} and k_{ca} the characteristic impedance and the characteristic wave-number of the air contained in the gap, the normal surface impedance Z_s of system composed of the screen and the air gap, at the abscissa $x = -d - h$ is (see Ref. 3 for example):

$$Z_s = Z_{cs}\frac{-jZ_{sp} + Z_{cs}\tan(k_{cs}h)}{Z_{sp}\tan(k_{cs}h) - jZ_{cs}} \tag{7}$$

where j is the square root of -1 and Z_{sp} is the surface impedance at $x = -d$ (i.e., interface between the screen and the air cavity)

$$Z_{sp} = -j\frac{Z_{ca}}{\tan(k_{ca}d)} \tag{8}$$

Visco-thermal dissipations in the air cavity can be included in expressions of Z_{ca} and k_{ca} using expressions given by trutt (Lord Rayleigh).[18] To avoid using these expressions based on the computation of Bessel functions one might alternatively use a JCA model with parameters $\sigma_a = 8\eta/R^2$, $\phi_a = 1$, $\alpha_{\infty a} = 1$, and $\Lambda_a = \Lambda'_a = R$ where R is the radius of the impedance tube.

At low frequencies $|k_{cs}h| \ll 1$ and $|k_{ca}d| \ll 1$ so that $\tan(k_{cs}h)$ and $\tan(k_{ca}d)$ reduce at the first order to $(k_{cs}h)$ and $(k_{ca}d)$, respectively. An approximate value of the frequency above which these conditions are no more verified can be obtained replacing k_{cs} and k_{ca} with the wave-number in free air. At such low frequencies and away from the frequency bands around acoustic cavity resonances given by Eq. (1), the normal surface impedance of the system can be approximated with

$$Z_s \simeq Z_{cs}\frac{-jZ_{sp} + Z_{cs}k_{cs}h}{-jZ_{cs}\left(1 + \frac{jZ_{sp}k_{cs}h}{Z_{cs}}\right)}. \tag{9}$$

Making use of Eq. (8) and the low frequency approximations, the fractional term at the denominator of Eq. (9), named hereafter A, can be re-written as:

$$A = \frac{Z_{ca}k_{cs}h}{k_{ca}Z_{cs}d} \tag{10}$$

From Eqs. (5) and (6) which are general expressions and can be applied to Z_{cs} as well as Z_{ca}, A reads:

$$A = \frac{K_{ca}h}{K_{cs}d} \tag{11}$$

The asymptotic limits for low and high frequencies of the bulk modulus of the screen K_{cs} are P_0/ϕ and $\gamma P_0/\phi$, respectively (γ is the ratio of the specific heats in air and P_0 refers to the static atmospheric pressure). These limits are, respectively, P_0 and γP_0 for the bulk modulus of the air in the cavity K_{ca}. Since the porosity of the screen ϕ is smaller than 1, K_{cs} is of the same order of magnitude or large compared to K_{ca}. Assuming the thickness of the screen is much smaller than the thickness of the air cavity ($h \gg d$), A is finally found to be negligible compared to 1 and Eq. (7) can be re-written as

$$Z_s \simeq Z_{sp} + j\omega\tilde{\rho}_{cs}h, \tag{12}$$

where ω denotes the angular frequency of the incident acoustic wave.

From Eq. (12), we deduced the expression of the screen dynamic mass density $\tilde{\rho}_{cs}$,

$$\tilde{\rho}_{cs} \simeq \frac{Z_s - Z_{sp}}{j\omega h} \tag{13}$$

The meaning of $\tilde{\rho}_{cs}$ is the same as for porous media: it represents the apparent mass density of the air in the screen. This value differs from its static real value of 1.2 kg m^{-3} due to visco-inertial effects inside the screen and due to the flow distortion effects on both sides of the screen.

When Z_s is measured, all quantities on the right hand side of Eq. (13) are known. Thus, $\tilde{\rho}_{cs}$ can be assessed.

The general expression of $\tilde{\rho}_{cs}$ given by Johnson *et al.*[7] is

$$\tilde{\rho}_{cs}(\omega) = \frac{\alpha_\infty\rho_0}{\phi}\left[1 - j\frac{\sigma\phi}{\omega\rho_0\alpha_\infty}\sqrt{1 + j\frac{4\alpha_\infty^2\eta\rho_0\omega}{\sigma^2\Lambda^2\phi^2}}\right]. \tag{14}$$

The low frequency expression of $\tilde{\rho}_{cs}$ obtained as the Taylor series of Eq. (14) at the first degree in ω reads

$$\tilde{\rho}_{cs}(\omega) = \frac{\alpha_\infty\rho_0}{\phi}\left(1 + \frac{2\alpha_\infty\eta}{\sigma\Lambda^2\phi}\right) - j\frac{\sigma}{\omega}, \tag{15}$$

which could also be re-written as

$$\tilde{\rho}_{cs}(\omega) = \frac{\alpha_\infty\rho_0}{\phi}\left(1 + \frac{\alpha_\infty}{4}\right) - j\frac{\sigma}{\omega}, \tag{16}$$

using the fact that $\sigma = 8\eta/(\phi r^2)$ and $\Lambda = r$ for the perforation geometry assumed.

On the one hand, it appears in Eq. (16) that the imaginary part of $\tilde{\rho}_{cs}$, $\mathrm{Im}(\tilde{\rho}_{cs})$, can be used to estimate the static air flow resistivity σ,

$$\sigma = -\omega\,\mathrm{Im}(\tilde{\rho}_{cs}) \tag{17}$$

On the other hand, the real part of Eq. (16) is given by

$$\mathrm{Re}(\tilde{\rho}_{cs}) = \frac{\alpha_\infty\rho_0}{\phi}\left(1 + \frac{\alpha_\infty}{4}\right) \tag{18}$$

with α_∞ given by Eqs. (3) and (4).

Equation (18) can be re-written as a polynomial expression of order 6 in $E = \sqrt{\phi}$ replacing α_∞ by its expression as a function of ϕ and r. r is then replaced by its expression as a function of ϕ and σ, $r = \sqrt{8\eta/(\sigma\phi)}$. Indeed σ is a parameter which can be directly measured [see ISO 9053 (Ref. 12)] or estimated from Eq. (17). The possible

values for E are then retrieved as roots of the polynomial. Only the real positive value contained in the open interval $]0-1[$ is physical. Finally, ϕ is calculated from the value of E as $\phi = E^2$. It should be highlighted here than among the numerous characterizations done by the authors only one admissible solution was found per screen. In the case of multiple admissible solutions, only one porosity value would correctly predict the acoustical behavior of the screen and, in particular, the normal sound absorption of the screen backed by an air gap. In this latter case, optical measurements can also be done to discriminate between possible solutions. For optical measurements of the porosity, a fine photography of the facing micro-structure is first obtained using, e.g., a magnifying glass. A color threshold is then applied to convert the color picture to a binary image (black and white image, for instance black for air and white for the facing skeleton). The porosity is then deduced from the ratio of the black-pixel count over the total-pixel count.

To check the consistency of characterization results, one might compare the simulations of the surface properties for the screen and air gap system to the measurements.

The surface impedance of the screen + air gap cavity system, Z_s, can be recovered from estimated parameters ϕ and r using its low frequency approximation [cf. Eq. (12)] and making use of the Eqs. (16), (3), and (4),

$$Z_s \simeq Z_{\mathrm{sp}} + j\omega\frac{\alpha_\infty\rho_0}{\phi}\left(1+\frac{\alpha_\infty}{4}\right)h + \sigma h \tag{19}$$

Alternatively, a transfer matrix method computation[19] with the complete JCA model to describe the screen layer can be used. In this latter case, Eq. (14) is used to express the dynamic mass density of the screen and Eq. (20) is used to express its dynamic bulk modulus.

$$\tilde{K}(\omega) = \frac{\gamma P_0/\phi}{\gamma-(\gamma-1)\left[1-j\frac{8\kappa}{\Lambda'^2 C_p\rho_0\omega}\sqrt{1+j\frac{\Lambda'^2 C_p\rho_0\omega}{16\kappa}}\right]^{-1}} \tag{20}$$

In the above expressions, C_p denotes the specific heat at constant pressure of the air, κ is the thermal conductivity of the air, and Λ', which refers to the thermal characteristic length of the screen, is equal to r.

The sound absorption coefficient α can be deduced from the normal surface impedance,

$$\alpha(\omega) = 1 - \left|\frac{Z_s(\omega)-Z_0}{Z_s(\omega)+Z_0}\right|^2, \tag{21}$$

where Z_0 is the characteristic impedance of air ($Z_0 = \rho_0 c_0$).

III. EXAMPLES OF CHARACTERIZATION

In Secs. III A and III B, we present characterization results for two screens. First, a woven screen is studied and the step-by-step procedure of the proposed characterization method is recalled. Second, a non-woven screen is studied. These screens represent two different types of facings which may be found in building or transport applications.

A. Example A: Low porosity, high resistivity screen

This first example is a highly resistive screen of surface mass density around 445 gm^{-2} and thickness 0.55 mm (cf. Fig. 2).

From direct measurements on screen samples (one material specimen per measurement), a mean value of this screen static air flow resistivity has been found to be equal to $775\,000 \pm 26\,900$ N s m^{-4}. The mean value leads to a high air flow resistance ($\sigma \times h$) of 426 N s m^{-3}, greater than the minimal resistance required to ensure a fair prediction of the static air flow resistivity by a direct measurement using ISO 9053.

Figure 3 presents the estimation result for the static air flow resistivity σ of the screen from Eq. (17). This estimation is based on the measurement of the surface impedance of the sample in the impedance tube with a 200 mm air cavity backing. A linear frequency scale has been used, as it appears more adequate to identify the one-dimensional resonances of the system composed by the screen and the air in the cavity [cf. Eq. (1)]. All results are reported including those around cavity mode resonances for which the denominator in Eq. (7) tends to 0 (so that the estimation of σ diverges). Obviously, the estimation of σ should be done using the results outside these frequency bands.

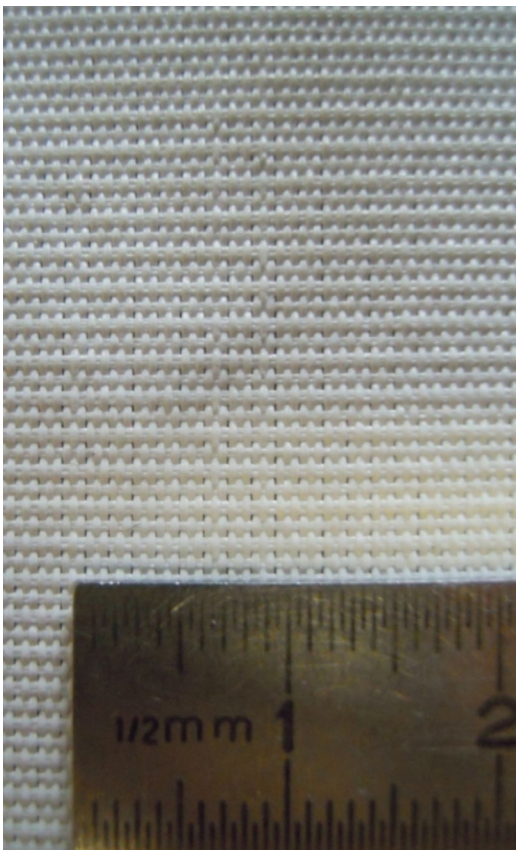

FIG. 2. (Color online) Close-up picture of a sample of woven fabric A. Fibers appear in white. At this scale, perforations cannot be clearly seen.

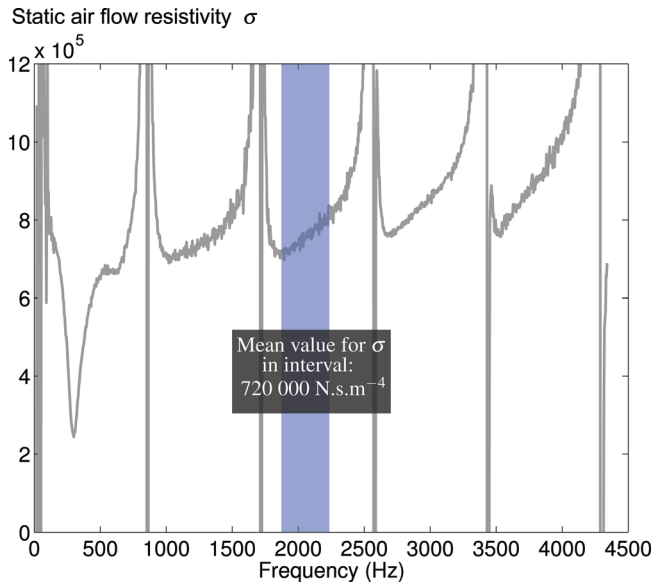

FIG. 3. (Color online) Estimation of static air flow resistivity for screen A from normal impedance measurement with a 200 mm air-gap and Eq. (17).

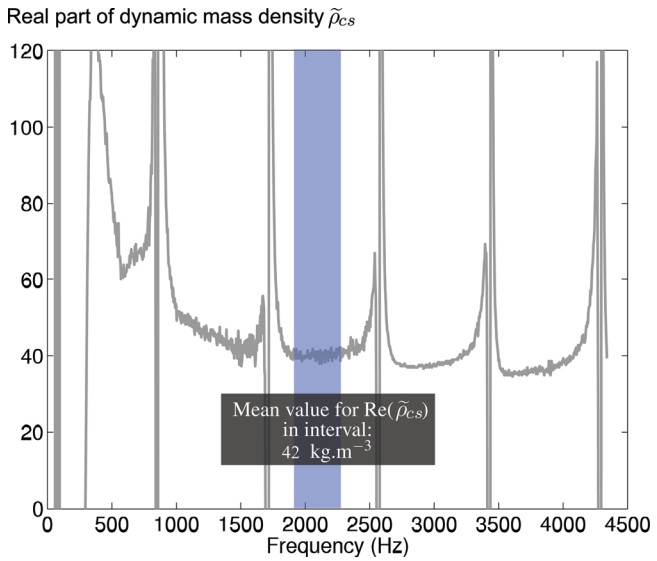

FIG. 4. (Color online) Estimation of the real part of the dynamic mass density $\tilde{\rho}_{cs}$ for screen A from normal impedance measurement with a 200 mm air-gap and Eq. (13).

It appears that the measurements are perturbed by the first vibrational mode of the screen around 300 Hz. Consequently, this frequency band should not be used to estimate σ.

Keeping in mind that the estimation should be done in the low frequency range for the condition $|k_{cs}h| \gg 1$ to be valid, only the measured data contained in the colored frequency band of Fig. 3 can be exploited. From this data, a mean value and a standard deviation for σ can be estimated, $720\,000 \pm 36\,800$ N s m^{-4}. This confidence interval overlaps the one obtained using direct measurements of σ. The mean value estimated with the current method differs from the measured one from 7%. The standard deviation is larger than the standard deviation observed for direct measurements using ISO 9053. However, this latter value represents a relative standard deviation of only 5%.

Figure 4 presents results obtained for the estimation of $\mathrm{Re}(\tilde{\rho}_{cs})$. The same observations as previously reported can be made concerning the assumption $|k_{cs}h| \gg 1$ and the first bending vibration of the screen.

An estimation of $\mathrm{Re}(\tilde{\rho}_{cs})$ is obtained from the mean value of the data contained in the same frequency band used for σ (cf. colored area in Fig. 4). The mean value is found to be 40 kg m^{-3} and the standard deviation is 2 kg m^{-3}.

From the mean values of σ and $\mathrm{Re}(\tilde{\rho}_{cs})$, the open-porosity and the perforation radius r are deduced, $\phi = 0.04$ and $r = 68 \times 10^{-6}$ m. α_∞ is found to be equal to 1.15. Note that this last value should be re-computed if the screen is used in another configuration (i.e., placed behind or above another porous material) to account for corresponding flow distortions.[6]

Finally, Fig. 5 presents a comparison between the measured sound absorption coefficient and the simulated one using the parameters characterized above. The studied configuration corresponds to plane waves under normal incidence impinging on the screen backed by a 200 mm air-gap. A good correspondence between measurements and simulation can be observed in all the studied frequency range. An underestimation of the dissipative effects in the cavity is mainly responsible for the deviation between the two curves at low values of the sound absorption which appear near cavity resonances.

Again, one can notice that measurements around 300 Hz are perturbed by the first bending resonance of the screen. Finally, at high frequencies, deviations between measurements and simulation are mainly due to the hypotheses of the model which become no more valid.

B. Example B: High porosity, low resistivity screen

The second example is a low resistivity screen of surface mass density around 60 gm^{-2} and thickness 0.35 mm (cf. Fig. 6). This non-woven screen is expected to have a higher open-porosity than screen A.

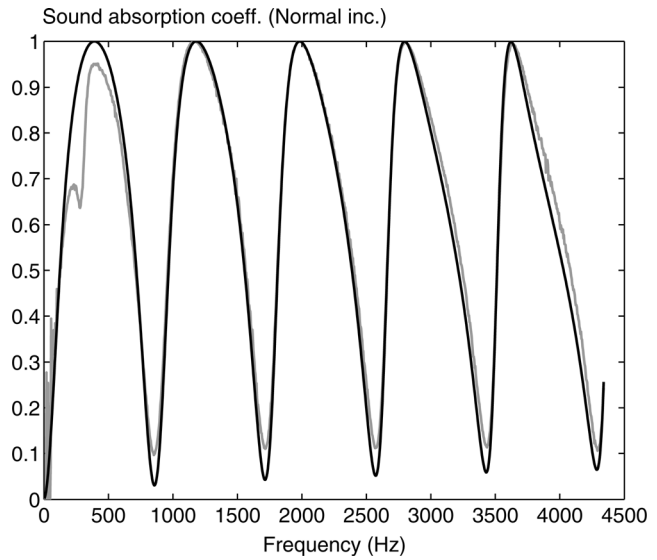

FIG. 5. Sound absorption coefficient at normal incidence, room temperature, and pressure conditions, for screen A with a 200 mm air-gap. Gray curve: measurements; black curve: simulation using estimated parameters from normal impedance measurements.

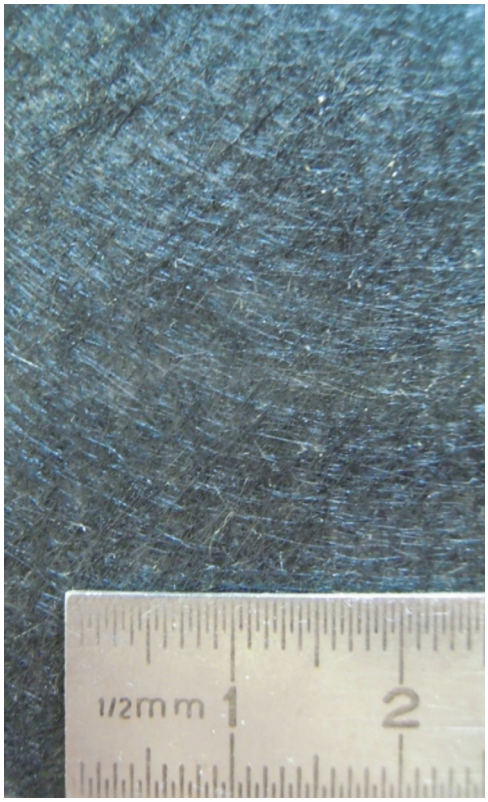

FIG. 6. (Color online) Close-up picture of a sample of non-woven fabric B. Fibers appear in black and perforations appear in light gray.

The static air flow resistivity of this second screen B being too low to be accurately measured with one sample using ISO 9053, several arrangements of six samples have been used. The measured value from these arrangements of samples is found to be equal to 99 000 ± 7400 N s m^{-4}. This mean value of σ, which leads to a low air flow resistance ($\sigma \times h$) of 35 N s m^{-3}, may be overestimated due to different fiber orientations between the six screen samples.

Following the steps described in the previous example, the static air flow resistivity of the screen is estimated, as the mean value of results in a frequency band is around 3000 Hz. This value, 87 000 N s m^{-4}, differs from the value directly measured by 14%. The standard deviation is found to be equal to 4400 N s m^{-4} (i.e., 5% of the mean value). Again, an overlap of the directly measured and estimated values is observed. The real part of the $\mathrm{Re}(\tilde{\rho}_{\mathrm{cs}})$ is then estimated in the same frequency band around 3000 Hz. The mean value obtained is equal to 2.1 kg m^{-3} while the standard deviation is equal to 0.1 kg m^{-3}. Finally, the only valid values for the open-porosity and the perforation radius are found to be equal to 0.72 and 48 × 10^{-6} m, respectively. This corresponds to a value for α_∞ of 1.02, which represents a low flow distortion coherent with a high porosity screen.

Figure 7 presents a comparison between the measured and the simulated normal sound absorption coefficient of the screen backed by a 200 mm air-gap.

Again, despite low values of the sound absorption near cavity resonances, which are not correctly predicted, a good correspondence between measurements and simulation is obtained in all the studied frequency range.

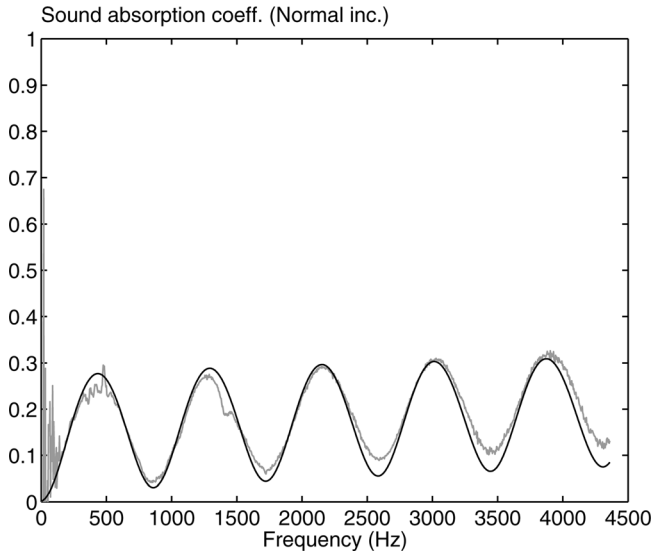

FIG. 7. Sound absorption coefficient at normal incidence, room temperature, and pressure conditions, for screen B with a 200 mm air-gap. Gray curve: measurements; black curve: simulation using estimated parameters from normal impedance measurements.

IV. CONCLUSION

A method to estimate the two independent acoustical parameters of perforated facings (also called screens), as modeled by Atalla and Sgard,[6] has been presented. These two parameters may be chosen out of a set of the three following ones: the perforation radius r, the perforation rate ϕ, and the static air flow resistivity σ. The proposed method is based (i) on the measurement of the surface impedance at normal incidence in a standing wave tube of a screen sample with an air gap of prescribed thickness and (ii) on the numerical determination of the roots of a polynomial of order 6 in $\sqrt{\phi}$.

A variant of the present method can be achieved by measuring directly the static air flow resistivity using an ISO standard. This either avoids the calculation of the static air flow resistivity or provides a reference measurement to check the parameters accuracy.

Characterization results have been presented for two different screens to test the validity and the accuracy of the method. The two screens represent high to low resistivities and low to high porosities. The estimated resistivity values are found to fall within the confidence interval of the directly measured results for both tested screens. Finally, the estimated parameters for each screen have been found to predict accurately its acoustical behavior in the frequency range [200−4500] Hz which corresponds to the main range of building and transportation applications.

ACKNOWLEDGMENT

Xavier Olny and Franck Sgard are greatly thanked for the fruitful discussions they had with the authors concerning acoustical porous materials and their characterizations.

[1]D. Y. Maa. "Microperforated wideband absorbers," Noise Control Eng. J. **29**(3), 77–84 (1987).
[2]L. L. Beranek, *Noise and Vibration Control Engineering* (Wiley, New York, 1992), Chap. 8.
[3]J.-F. Allard, *Propagation of Sound in Porous Media. Modeling Sound Absorbing Materials* (Elsevier Applied Sciences, London, New York, 1993), Chap. 10, pp. 220–253.
[4]K. U. Ingard, *Notes on Sound Absorption Technology* (Noise Control Foundation, Poughkeepsie, NY, 1994), Chap. 2, pp. 2–1 to 2–35.
[5]K. Sakagami, M. Kiyama, M. Morimotoc, D. Takahashi, S. Kimihiro, K. Masakazu, M. Masayuki, and D. Takahashid, "Detailed analysis of the acoustic properties of a permeable membrane," Appl. Acoust. **54**(2), 93–111 (1998).
[6]N. Atalla and F. Sgard, "Modeling of perforated plates and screens using rigid frame porous models," J. Sound Vib. **303**, 195–208 (2007).
[7]D. L. Johnson, J. Koplik, and R. Dashen, "Theory of dynamic permeability and tortuosity in fluid-saturated porous media," J. Fluid Mech. **176**, 379–402 (1987).
[8]Y. Champoux and J.-F. Allard, "Dynamic tortuosity and bulk modulus in air-sturated porous media," J. Appl. Phys. **70**, 1975–1979 (1991).
[9]O. C. Zwikker and C. W. Kosten, *Sound-Absorbing Materials* (Elsevier, New York, 1949), Chap. 4, pp. 76–84.
[10]Y. Champoux, M. R. Stinson, and G. A. Daigle, "Air-based system for the measurement of porosity," J. Acoust. Soc. Am. **89**(2), 910–916 (1991).
[11]Ph. Leclaire, O. Umnova, K. Horoshenkov, and L. Maillet, "Porosity measurement by comparison of air volumes," Rev. Sci. Instrum.**74**(3), 1366–1370 (2003).
[12]International Organization for Standardization (ISO). *Acoustics—Materials for Acoustical Applications—Determination of Airflow Resistance* (ISO, Geneva, Switzerland, 1991).
[13]R. Panneton, "Comments on the limp frame equivalent fluid model for porous media," J. Acoust. Soc. Am. **122**(6), EL217 (2007).
[14]F.-X. Bécot and F. Sgard, "On the use of poroelastic materials for the control of the sound radiated by a cavity backed plate," J. Acoust. Soc. Am. **120**(4), 2055–2066 (2007).
[15]M. A. Biot, "Theory of propagation of elastic waves in a fluid-saturated porous solid. I. Low-frequency range," J. Acoust. Soc. Am. **28**(2), 168–178 (1956).
[16]M. A. Biot, "Theory of propagation of elastic waves in a fluid-saturated porous solid. II. Higher frequency range," J. Acoust. Soc. Am. **28**(2), 179–191 (1956).
[17]A. W. Leissa, *Vibration of Plates* (Acoustical Society of America, Sewickley, 1993), pp. 7–35.
[18]J. W. Strutt, *The Theory of Sound, Vol. 2* (Dover Publications Inc., New York, 1945), Chap. 16, pp. 170–235.
[19]B. Brouard, D. Lafarge, and J.-F. Allard, "A general method of modelling sound propagation in layered media," J. Sound Vib. **183**(1), 129–142 (1995).